

# Lawrence Berkeley National Laboratory

## Recent Work

### Title

Integrated cooling (i-Cool) textile of heat conduction and sweat transportation for personal perspiration management.

### Permalink

<https://escholarship.org/uc/item/259001jv>

### Journal

Nature communications, 12(1)

### ISSN

2041-1723

### Authors

Peng, Yucan  
Li, Wei  
Liu, Bofei  
[et al.](#)

### Publication Date

2021-10-01

### DOI

10.1038/s41467-021-26384-8

Peer reviewed

1           **Integrated Cooling (i-Cool) Textile of Heat Conduction and Sweat**  
2           **Transportation for Personal Perspiration Management**

3 Yucan Peng<sup>1†</sup>, Wei Li<sup>2,3†</sup>, Bofei Liu<sup>1</sup>, Weiliang Jin<sup>2</sup>, Joseph Schaad<sup>4,5</sup>, Jing Tang<sup>1</sup>, Guangmin Zhou<sup>1</sup>,  
4 Guanyang Wang<sup>6</sup>, Jiawei Zhou<sup>1</sup>, Chi Zhang<sup>7</sup>, Yangying Zhu<sup>1</sup>, Wenxiao Huang<sup>1</sup>, Tong Wu<sup>1</sup>, Kenneth  
5 E. Goodson<sup>7</sup>, Chris Dame<sup>4,5</sup>, Ravi Prasher<sup>4,5</sup>, Shanhui Fan<sup>2</sup> & Yi Cui<sup>1,8\*</sup>

6     <sup>1</sup>Department of Materials Science and Engineering, Stanford University, Stanford, CA 94305, USA.

7     <sup>2</sup>E. L. Ginzton Laboratory, Department of Electrical Engineering, Stanford University, Stanford, CA  
8     94305, USA.

9     <sup>3</sup>GPL Photonics Lab, State Key Laboratory of Applied Optics, Changchun Institute of Optics, Fine  
10    Mechanics and Physics, Chinese Academy of Sciences, Changchun, 130033, China.

11    <sup>4</sup>Department of Mechanical Engineering, University of California, Berkeley, CA 94720, USA

12    <sup>5</sup>Energy Technologies Area, Lawrence Berkeley National Laboratory, 1 Cyclotron Road, Berkeley,  
13    CA 94720, USA

14    <sup>6</sup>Department of Mathematics, Stanford University, Stanford, CA 94305, USA

15    <sup>7</sup>Department of Mechanical Engineering, Stanford University, Stanford, CA 94305, USA.

16    <sup>8</sup>Stanford Institute for Materials and Energy Sciences, SLAC National Accelerator Laboratory,  
17    2575 Sand Hill Road, Menlo Park, CA 94025, USA.

18    <sup>†</sup>These authors contributed equally to this work

19    \*Corresponding author: Yi Cui (yicui@stanford.edu)

20  
21    **Abstract**

22    **Perspiration evaporation plays an indispensable role in human body heat dissipation.**  
23    **However, conventional textiles tend to focus on sweat removal and pay little attention to the**  
24    **basic thermoregulation function of sweat, showing limited evaporation ability and cooling**  
25    **efficiency in moderate/profuse perspiration scenarios. Here, we propose an integrated**

26 cooling (i-Cool) textile with unique functional structure design for personal perspiration  
27 management. By integrating heat conductive pathways and water transport channels  
28 decently, i-Cool exhibits enhanced evaporation ability and high sweat evaporative cooling  
29 efficiency, not merely liquid sweat wicking function. In the steady-state evaporation test,  
30 compared to cotton, up to over 100% reduction in water mass gain ratio, and 3 times higher  
31 skin power density increment for every unit of sweat evaporation are demonstrated. Besides,  
32 i-Cool shows about 3 °C cooling effect with greatly reduced sweat consumption than cotton  
33 in the artificial sweating skin test. The practical application feasibility of i-Cool design  
34 principles is well validated based on commercial fabrics. Owing to its exceptional personal  
35 perspiration management performance, we expect the i-Cool concept can provide promising  
36 design guidelines for next-generation perspiration management textiles.

37

## 38 **Introduction**

39 Satisfaction with the thermal environment for human body is significant, not merely due to the  
40 demand for comfort, but more importantly because thermal conditions are crucial for human body  
41 health<sup>1</sup>. Heat-resulted physiological and psychological problems not only can be threatening for  
42 human health<sup>2</sup>, but also negatively influence labor productivity and society economy<sup>3</sup>. Personal  
43 thermal management focusing on thermal conditions of human body and its local environment is  
44 emerging as an energy-efficient and cost-effective solution<sup>4,5</sup>. Without consuming excess energy  
45 on managing the temperature of the entire environment<sup>6,7</sup>, innovative textiles have been designed  
46 for controlling human body heat dissipation routes<sup>8,9</sup>. In general, human body dissipates heat via  
47 four different pathways: radiation, convection, conduction and evaporation<sup>10</sup>. Recently, textiles  
48 with engineered radiative properties<sup>11-16</sup>, convective and conductive properties<sup>17-19</sup> have been  
49 demonstrated as promising approaches for personal thermal management especially for mild  
50 scenarios. However, for intense scenarios, textiles for ideal personal perspiration or evaporation  
51 management are still lacking.

52 For the delicate human body system with a narrow temperature range (36 – 38 °C core temperature  
53 at rest and up to 41°C for heavy exercise)<sup>20</sup>, evaporation plays an indispensable role in human  
54 body thermoregulation. Even at a mild state, about 20 percent of heat dissipation of the dry human

55 body relies on the water vapour loss via insensible perspiration<sup>10,21</sup>. With further increase of heat  
56 load, liquid sweat evaporation contributes to more and more heat loss and becomes the major route  
57 for human body heat dissipation in intense scenarios such as heavy exercise and hot/humid  
58 environments, where excess heat cannot be dissipated efficiently by other pathways<sup>22,23</sup>. State-of-  
59 the-art textiles for daily use are usually sufficiently good at water vapour transmission to ensure  
60 comfort at the mild state (See Supplementary Note 1 and Supplementary Fig. 1-2 for more  
61 discussion)<sup>24</sup>. Nevertheless, the cooling performance of conventional textiles is to be improved  
62 when human body is in more intense scenarios, such as moderate/profuse perspiration situations  
63 in which liquid sweat is inevitably present.

64 In order to avoid increased wettedness on the skin which causes less comfort in such cases<sup>25,26</sup>,  
65 state-of-the-art textiles, including moisture management fabrics, tend to focus on sweat removal.  
66 Textiles made of natural fibres, such as cotton, show strong water absorption capacity, which can  
67 help alleviate sense of wettedness quickly<sup>27</sup>. In spite of diminished absorbing ability, synthetic  
68 fibres (with profiled cross-section), such as polyester, are developed to possess enhanced moisture  
69 transportation than natural fibres to deliver water to the textile surface for faster evaporation<sup>28,29</sup>.  
70 Microfibres are also explored for improved wicking<sup>30</sup>. Besides, strategies including surface  
71 hydrophilicity/hydrophobicity modification<sup>31-33</sup>, multiple-layer design with differential  
72 wettability<sup>34,35</sup> and hierarchical design of multiscale interconnected pores with capillarity  
73 gradient<sup>36,37</sup> are reported to realize better controlled directional water transportation. These textiles  
74 serve as a buffer absorbing water to provide dry sense for people and can potentially offer a  
75 comparatively larger surface area for evaporation.

76 However, how to efficiently unlock the cooling power of sweat evaporation for human body  
77 thermoregulation and design textiles based on laws of human body perspiration process have not  
78 been taken into account. In the aspect of thermoregulation, sweat is secreted to be evaporated and  
79 take away the excess heat. Nevertheless, although sweat evaporation does happen on the  
80 conventional textiles, human skin underneath is not effectively cooled since heat for vaporization  
81 is not efficiently drawn from the skin because of the limited heat transfer<sup>38-40</sup>. One extreme case  
82 is that only the textile surface rather than human skin can be cooled. In other words, the sweat  
83 absorbed in the conventional textiles shows decreased evaporative cooling efficiency in cooling  
84 the human body, which means sweat is less efficiently utilized. Also, even regarding evaporation

85 rate of conventional textiles, it is relatively restrained because skin heat cannot be efficiently  
86 delivered to the evaporation interface to accelerate evaporation. The inefficient cooling effect will  
87 lead to further perspiration, and meanwhile the slow sweat evaporation, will result in the  
88 accumulation of sweat in the textile. This process may undermine the buffer effect of the textiles  
89 once the absorption limit of the fabric is reached, at which point the human body will get wet and  
90 sticky again. The excessive perspiration can also cause potential risk of dehydration, electrolyte  
91 disorder, physical and mental deterioration or even death<sup>41</sup>. Moreover, when people are in highly  
92 active scenarios, the maximum cooling power of sweat evaporation that can be achieved actually  
93 limits the maximum activity level of human body<sup>42</sup>. Accordingly, in addition to decent wicking  
94 property, an optimal textile for perspiration scenario should show high evaporation ability and  
95 more importantly high sweat evaporative cooling efficiency to utilize sweat in a highly efficient  
96 manner, to provide adequate cooling effect using minimized amount of sweat.

97 In this work, we propose a novel concept of integrated cooling (i-Cool) textile of heat conduction  
98 and sweat transportation to achieve the as-mentioned goals based on human body perspiration  
99 process, as illustrated in Fig. 1a. We introduce heat conductive components into the textile and  
100 divide the functionalities of heat conduction and sweat transport into two operational components.  
101 The heat conductive matrix and sweat transportation channels are integrated together in the i-Cool  
102 textile. The synergistic effect of the two components results in excellent performance at sweat  
103 wicking, fast evaporation, efficient evaporative cooling for human body and reducing human body  
104 dehydration. As shown in Fig. 1b, the sweat transport channels can pull liquid water up from skin  
105 and spread it out in the sweat transport channels for evaporation. On the other hand, the heat  
106 conductive matrix can efficiently transfer skin heat to the evaporation spots that are integrated on  
107 the heat conductive matrix<sup>43,44</sup>. Therefore, combined with large evaporation area and efficient heat  
108 conduction from skin, sweat absorbed in the water transportation channels can be evaporated  
109 quickly into air, taking away a huge amount of heat from the skin. The efficient heat removal from  
110 the skin provides improved evaporative cooling effect and decrease skin temperature effectively,  
111 which will consequently reduce human body dehydration. As illustrated in Fig. 1c, compared to  
112 the conventional textiles, the i-Cool textile functions not only to wick sweat but also provide heat  
113 conduction paths for the accelerated evaporation and efficiently take away a great amount of heat  
114 from the skin. Furthermore, the enhanced evaporation ability and high sweat evaporative cooling  
115 efficiency can prevent the i-Cool textile from flooding to a much greater extent and avoid excessive

116 perspiration. The improved evaporative cooling effect does not mean more sweat needs to be  
117 generated or even evaporated. Therefore, the i-Cool textile can help human body achieve enhanced  
118 cooling effect with greatly reduced sweat secretion by using the sweat in a highly efficient manner.

## 119 **Results and discussion**

120 On the basis of the i-Cool functional structure design principles as outlined above, we selected  
121 copper (Cu) and nylon 6 nanofibres for proof of concept. It is worthwhile to mention that Cu and  
122 nylon 6 nanofibres are not the only choices. Other materials satisfying the design principles can  
123 be applied as well. Here, Cu is well-known for its extraordinary thermal conductivity ( $\sim 400 \text{ W}\cdot\text{m}^{-1}\cdot\text{K}^{-1}$ ),  
124 and nylon 6 nanofibres are capable of water wicking. As illustrated in Supplementary Fig.  
125 3, electrospinning was utilized to generate nylon 6 nanofibres, which were transferred to the heat  
126 conductive Cu matrix prepared by laser cutting. With press lamination, the i-Cool (Cu) textile with  
127 desired functional structure design was fabricated. The photograph of as-fabricated i-Cool (Cu)  
128 textile is displayed in Fig. 2a. Nylon 6 nanofibres not only cover the Cu top surface, but also fill  
129 inside the pores, as shown in the magnified photograph of the bottom side of the i-Cool (Cu) textile  
130 in the inset of Fig. 2b. Nanofibres on the skeleton of Cu matrix are denser with smaller void space  
131 among the nanofibres than the ones in the pores of Cu matrix, which can be clearly observed in  
132 the scanning electron microscope (SEM) images in Fig. 2b and Supplementary Fig. 4. The  
133 capillarity difference resulted from the morphology difference benefits one-way directional water  
134 transportation from inner surface to outer surface. To evaluate the performance of the i-Cool (Cu)  
135 textile, we selected cotton textile as the main control textile since it is arguably the most widely  
136 used and accepted textile in human history. We have also chosen other well-known activewear  
137 fabrics for comparison purposes.

### 138 **Liquid water transport characterization**

139 Textiles designed for perspiration scenarios must be able to wick sweat from the skin (in contact  
140 with textile bottom) and spread it out. Correspondingly, we tested in parallel the i-Cool (Cu) textile  
141 and commercial textiles including cotton, Dri-FIT, CoolMax and Coolswitch via mimicking the  
142 sweat transport process from the human body skin to the outer surface of the textile. Textile  
143 samples covered a certain amount of liquid water on the platform respectively, and the wicking  
144 rate was calculated via dividing wicking area by wicking time for every sample (Supplementary

145 Fig. 5). It turned out that the interconnected nylon 6 nanofibres in the i-Cool (Cu) textile was able  
146 to quickly transport liquid water from bottom to top and spread it out, which exhibited comparable  
147 or higher wicking rate in comparison with conventional textiles (Fig. 2c). Besides, due to the  
148 unique structure design and the nanofibre morphology variation from i-Cool (Cu) bottom to the  
149 outer surface, i-Cool (Cu) exhibits good one-way water transport property. As displayed in  
150 Supplementary Fig. 6a, the water droplet added onto the inner side of i-Cool (Cu) can be  
151 transported to the outer surface and spread out very quickly while little water remained on the  
152 inner side. In reverse, water transportation was limited when the water droplet added to the outer  
153 side. As a comparison, for cotton, the water spreading area on the outer side and inner side was  
154 almost the same no matter which side the water droplet was added onto (Supplementary Fig. 6b),  
155 which means the conventional cotton fabric shows no one-way transport capability. Also, in the  
156 scenario of adding water onto inner side, the water spreading rate on the inner surface and outer  
157 surface ( $S_{\text{inner}}$  and  $S_{\text{outer}}$ ) and one-way transport index ( $\mu$ ) were defined and plotted in  
158 Supplementary Fig. 7<sup>45</sup>. The i-Cool (Cu) shows obviously different  $S_{\text{inner}}$  and  $S_{\text{outer}}$ , and very  
159 large  $\mu$ , while  $S_{\text{inner}}$  and  $S_{\text{outer}}$  are very similar for cotton and its  $\mu$  is very close to 1, which  
160 demonstrates the apparent one-way sweat transport advantage of i-Cool (Cu) again. This property  
161 can also help faster evaporation, because sweat can spread on the outer surface quickly and liquid  
162 water transport to the nanofibres right on the heat conductive Cu matrix is preferential<sup>37</sup>.

### 163 **Thermal resistance measurement**

164 To quantify the enhancement of heat transport capability of the i-Cool (Cu) textile, we performed  
165 the measurement of thermal resistance using cut bar method, as illustrated in Supplementary Fig.  
166 8. Using this method, we measured the dry thermal resistance of the i-Cool (Cu) textile and other  
167 commercial textile samples all under an additional contact pressure of ~15 psi (103 kPa). As  
168 exhibited in Fig. 2d, the i-Cool (Cu) textile shows about 14 – 20 times lower thermal resistance  
169 compared to the conventional textiles (See Supplementary Note 2 and Supplementary Fig. 8 for  
170 more details and discussion). A thermal resistor model was built up to interpret the measured  
171 thermal resistance. It was found out the nylon 6 nanofibre layer contributes to the major thermal  
172 resistance, and increasing the thickness of heat conductive matrix (Cu) will only cause minor  
173 increase of thermal resistance (Supplementary Fig. 9). It provides support for the possibility of  
174 extending the i-Cool concept into fabrics of various thickness.

## 175 **Transient droplet evaporation test**

176 We further used a transient droplet evaporation test to compare the evaporation performance of  
177 the i-Cool (Cu) textile and the conventional textiles. Figure 2e illustrates the experimental setup:  
178 A heater placed on an insulating foam was used to simulate human skin with a thermocouple  
179 attached to the heater surface; We added liquid water at 37 °C to mimic sweat onto the artificial  
180 skin, then textile samples covered on the wet artificial skin immediately; The power density of the  
181 artificial skin was maintained constant during the measurement. During the whole evaporation  
182 process, skin temperature was always monitored and recorded. For example, a group of typical  
183 curves of skin temperature versus time are shown in Supplementary Fig. 10. Generally, the curves  
184 can be divided into three stages for the tested textile samples. Initially, when water was just added  
185 onto the artificial skin, skin temperature dropped sharply. Then, skin temperature was relatively  
186 stable only fluctuating in a small range in the evaporation stage. Eventually, skin temperature rose  
187 again quickly once water was completely evaporated.

188 Two pieces of important information can be obtained through comparing the curves of i-Cool (Cu)  
189 and the conventional textiles. Firstly, the evaporation time with i-Cool (Cu) was much shorter,  
190 which indicates that i-Cool (Cu) exhibits higher evaporation rate. This conclusion can also be  
191 verified by measuring the mass loss of liquid water over time during the evaporation test  
192 (Supplementary Fig. 11). Secondly, skin temperature with i-Cool (Cu) textile was lower than the  
193 conventional textiles during evaporation, demonstrating human body can evaporate sweat faster  
194 with even lower skin temperature when a person wears i-Cool textile. The summarized comparison  
195 of average skin temperature and average evaporation rate between the i-Cool (Cu) textile and the  
196 conventional textiles is displayed in Fig. 2f (0.1 mL initial water, 422.5 W/m<sup>2</sup> power density,  
197 ambient temperature: ~ 22 °C). The i-Cool (Cu) shows 2.3-4.5 °C lower average skin temperature  
198 and about twice faster average evaporation rate compared to the conventional textiles.

199 Furthermore, measurements under assorted skin power density and initial liquid water amount for  
200 i-Cool (Cu) and cotton were performed. With different experimental parameters, the average  
201 evaporation rate was calculated and plotted versus the average skin temperature during evaporation  
202 in Supplementary Fig. 12a and Supplementary Fig. 12b. In our measurement range, a linear  
203 relationship between the average evaporation rate and the average skin temperature was observed  
204 with a certain amount of initial water. Employed the linear fitting relationship and replotted from



205 Supplementary Fig. 12, Fig. 2g shows the fitted relationship between the average evaporation rate  
206 and the initial water amount at different skin temperatures for the i-Cool (Cu) and cotton. Generally,  
207 the average evaporation rate increases as the initial water amount increases and it shows an  
208 approaching saturation trend as the initial water amount reaches a certain level. This is perhaps  
209 consistent with the change trend of average evaporation area during the drying process when the  
210 initial water amount is changed. It is obvious that the i-Cool (Cu) exhibits overall higher  
211 evaporation rate than cotton. Besides, i-Cool (Cu) can achieve this with lower initial water amount  
212 and lower skin temperature, indicating the superiority in sweat evaporation of the i-Cool functional  
213 structure design.

#### 214 **Steady-state evaporation test**

215 In order to further characterize the evaporation features of i-Cool (Cu) and analyze its advantages  
216 over conventional textiles, we performed a steady-state evaporation test. Compared to the transient  
217 droplet evaporation test above, the steady-state evaporation test can help derive more useful  
218 indexes to differentiate the evaporation property of textiles during human body perspiration. The  
219 measurement apparatus is illustrated in Fig. 3a. Similarly, a heater placed on an insulating foam  
220 was used to simulate human skin. Thermocouples and a water inlet which were sealed in a thin  
221 acrylic board were attached to the artificial skin surface. Not adding a certain initial amount of  
222 water, water heated to 37 °C was pumped onto the skin surface at a specific rate continuously, and  
223 textiles on it wicked the intake water. Power density of the skin was adjusted to maintain skin  
224 temperature stay at 35 °C. The system with textile samples finally reached a steady-state. By  
225 changing steady-state evaporation rate (i. e. water pumping rate), the corresponding stable water  
226 mass gain and power density can be measured for different textiles.

227 Figure 3b exhibits the measured water mass gain ratio (i. e. water mass gain/textile sample dry  
228 mass\*100%, denoted as  $W$ ) of i-Cool (Cu), cotton and Dri-FIT versus increasing evaporation rate  
229 (denoted as  $v$ ). Firstly, it was observed that the water mass gain ratio of i-Cool (Cu) was always  
230 lower than cotton and Dri-FIT at the same evaporation rate, indicating that less sweat is required  
231 to “activate” i-Cool (Cu) to reach the same evaporation rate compared to the conventional ones.  
232 For example, when the steady-state evaporation rate was 1.1 mL/h, i-Cool (Cu) only showed about  
233 20 percent of water mass gain ratio, while  $W$  of cotton was approximately 130 percent. This  
234 phenomenon was also in accordance with the transient droplet evaporation test results.

235 Furthermore, we fitted the curves in Fig. 3b and calculated water mass gain ratio gradient ( $dW/dv$ ),  
236 as shown in Fig. 3c.  $dW/dv$  of i-Cool (Cu) is apparently smaller than the conventional textiles, even  
237 if all of them displayed water mass gain increase as the growth of evaporation rate. Besides,  $dW/dv$   
238 of cotton and Dri-FIT rises rapidly with the increase of evaporation rate, especially cotton. It means  
239 that it becomes even more and more difficult to achieve higher evaporation rate. Nevertheless, this  
240 index for i-Cool (Cu) stays almost unchanged in the measurement range. During real human body  
241 perspiration, these features of i-Cool (Cu) enables it to fast evaporate sweat before sweat  
242 accumulates a lot and to retain a relatively dry state even during very profuse perspiration that  
243 requires high evaporation rate.

244 The measured power density (denoted as  $q$ ) of artificial skin in this test is shown in Fig. 3d. Overall,  
245 the skin power density with i-Cool (Cu) was higher than the conventional textiles when they were  
246 at the same evaporation rate, demonstrating the cooling ability of i-Cool (Cu) during perspiration  
247 is stronger. It is worthwhile to mention that i-Cool (Cu) is easier to reach higher evaporation rate,  
248 thus the cooling power difference between i-Cool (Cu) and conventional textiles may be enlarged.  
249 Besides, the curves in Fig. 3d were fitted and power density gradient ( $dq/dv$ ) could be derived, as  
250 displayed in Fig. 3e. This index ( $dq/dv$ ) exhibits the cooling power increment speed when  
251 evaporation rate increases. Obviously,  $dq/dv$  of i-Cool (Cu) is much higher than cotton and Dri-  
252 FIT, which means i-Cool (Cu) can provide much higher cooling power when every unit of sweat  
253 evaporates. To be specific,  $dq/dv$  of i-Cool (Cu) is about 3 times higher than that of cotton and Dri-  
254 FIT. Furthermore, to some extent,  $dq/dv$  can be converted into sweat evaporative cooling  
255 efficiency (denoted as  $\eta$ ) (See Supplementary Note 3 for more discussion). Based on our estimation,  
256 the evaporative cooling efficiency of i-Cool (Cu) is  $0.8 \sim 1$ , while  $\eta$  of cotton and Dri-FIT is only  
257  $0.2 \sim 0.4$  (Supplementary Fig. 13). Therefore, we demonstrated i-Cool (Cu) shows evident  
258 advantages in both evaporation ability and sweat evaporative cooling efficiency, which makes it  
259 to be promising in next-generation textiles for personal perspiration management.

## 260 **Artificial sweating skin platform with feedback control loop**

261 Human body is capable of adjusting itself to maintain homeostasis in the means of feedback control  
262 loops<sup>46</sup>. Taking perspiration as an example, when the human body temperature exceeds a threshold,  
263 the sympathetic nervous system stimulates the eccrine sweat glands to secrete water to the skin

264 surface. In reverse, water evaporation on the skin surface accelerates heat loss and thus body  
265 temperature decreases, which will reduce or suspend the perspiration of human body (Fig. 4a)<sup>47,48</sup>.

266 To mimic human body perspiration situation and show the performance difference between the i-  
267 Cool (Cu) textile and the conventional textiles, we designed an artificial sweating skin platform  
268 with feedback control loop, as illustrated in Fig. 4b. In this system, an artificial sweating skin that  
269 can generate sweat uniformly from every fabricated perspiration spot was built up and served as  
270 the test platform. Power was supplied to the artificial sweating skin platform to generate heat flux  
271 simulating human body metabolic heat. A syringe pump and a temperature controller were utilized  
272 to provide continuous liquid water supply at a constant temperature (37 °C) for the artificial  
273 sweating skin. A thermocouple was attached to the artificial sweating skin platform surface,  
274 monitoring skin temperature with a thermocouple meter that transmitted skin temperature data to  
275 the computer in real time. Subsequently, the internal set program could instantly alternate the  
276 pumping rate of the syringe pump that corresponds to the sweating rate of artificial sweating skin,  
277 which realized the feedback control loop imitating human body's feedback control mechanism.

278 To achieve uniform water outflow through each artificial sweat pore mimicking human body skin  
279 sweating, we designed the artificial sweating skin platform as illustrated in Fig. 4c. In the bottom,  
280 an enclosed small cuboid cavity connecting to water inlet acted as a water reservoir. When water  
281 was pumped in, water in the reservoir was forced out upwards through the channels on the reservoir  
282 cap. On the top of it, a perforated hydrophilic heater was attached to generate heat, in the meantime  
283 through which water can flow out. The uniform "sweating" from each artificial sweat pore was  
284 realized by the fabricated Janus-type wicking layer with limited water outlets that was placed  
285 above the perforated heater (See Supplementary Note 4 - 5 and Supplementary Fig. 14-16 for more  
286 details and discussion).

287 We believe that the measurement results obtained with the as-built artificial sweating skin platform  
288 can provide reasonable parallel thermal comparison among the textile samples, even though this  
289 set-up cannot fully represent the human body due to the lack of some other feedback control  
290 mechanisms such as blood flow feedback control and the differences in size, shape, thermal  
291 capacity, etc. With the realization of scale-up, we expect to conduct the human physiological wear  
292 experiment<sup>42</sup> in the near future.

### 293 **Artificial sweating skin test**

294 On the artificial sweating skin platform, we first performed a demonstrative experiment to  
295 intuitively show the sweat evaporative cooling efficiency difference. In this experiment, the same  
296 power density was used for the i-Cool (Cu) textile and cotton textile while the sweating rate was  
297 varied for different ones to realize the same skin temperature (34.5 °C), then we observed the  
298 condition of the artificial skin device and the textile samples after stabilization of 30 minutes. As  
299 shown in Supplementary Fig. 17, bare skin remained almost dry. The skin with the i-Cool (Cu)  
300 textile also remained dry while there was a little water absorbed in the sample. Nevertheless, there  
301 was a much larger amount of water remaining on both the skin platform and the cotton textile.  
302 These results intuitively demonstrated the i-Cool (Cu) can cool down the skin more efficiently  
303 consuming much less sweat.

304 Then, we performed measurements with constant skin power density for i-Cool (Cu) and other  
305 commercial textile samples, to mimic an exercise scenario of human body (See Supplementary  
306 Note 6 and Supplementary Fig. 18 for more discussion for this measurement). All the  
307 measurements were performed from the same initial state. The skin temperature and sweating rate  
308 (i.e. water pumping rate) after stabilization were measured. Figure 4d shows the experimental  
309 results when skin power density was  $\sim 750 \text{ W/m}^2$  and ambient temperature was 22 °C. The cooling  
310 performance of i-Cool (Cu) is very similar to the bare skin, which is recognized as the most  
311 efficient cooling approach since sweat evaporation can directly take away heat from the skin.  
312 Compared to the conventional textiles, i-Cool (Cu) exhibited evidently lower skin temperature ( $\sim$   
313 2.8 °C lower than cotton,  $\sim 2$  °C temperature difference with Dri-FIT and Coolswitch,  $\sim 3.4$  °C  
314 temperature difference with CoolMax). The sweating rate provided for the conventional textiles  
315 was over 2 – 3 times as much as i-Cool (Cu). It proves that conventional textiles cannot achieve  
316 better cooling effect even with much more available sweat. On the other hand, i-Cool (Cu) is able  
317 to unlock the cooling power of sweat more efficiently, which can deliver improved cooling effect  
318 with reduced sweating dehydration. As a result, conventional textiles would become highly wet  
319 after perspiration, whereas i-Cool (Cu) could retain a much drier state (insets of Fig. 4d), which is  
320 a comprehensive effect of evaporation ability and sweat evaporative cooling efficiency.

321 We tested the Cu heat conductive matrix and nylon 6 nanofibre film separately. The departure of  
322 the heat conduction component and water transport component makes both of them less efficient  
323 in evaporative cooling, as exhibited in Supplementary Fig. 19. These tests illustrate the key factor

324 to achieve an effective cooling effect is the integrated functional design of heat conduction and  
325 sweat transportation. Different cotton samples with various area mass density were also tested (See  
326 Supplementary Note 7 and Supplementary Fig. 20 for more details). In our experiments, the  
327 thinnest cotton sample ( $26.5 \text{ g/m}^2$ ) that is too transparent to be practically used still exhibited  
328 around  $1.5 \text{ }^\circ\text{C}$  higher skin temperature than the i-Cool (Cu) textile. These results further validate  
329 the superiority of the i-Cool structure that is an integrated one with both heat conduction and sweat  
330 transportation.

331 The artificial sweating tests under different skin power densities to simulate changed human body  
332 metabolic heat production were also conducted. As displayed in Fig. 4e, the enhanced cooling  
333 performance showing lower skin temperature and reduced sweating rate in comparison to  
334 conventional textiles was still true when different skin power densities were applied. It verifies the  
335 advantages of i-Cool in a wide range of heat production.

336 Besides, the evaluation of performance under diverse ambient environment conditions was  
337 performed, especially in high temperature circumstances and high relative humidity surroundings  
338 in which perspiration is more likely to happen. At the ambient temperature of  $40 \text{ }^\circ\text{C}$ , the  
339 evaporative cooling performance of i-Cool (Cu) textile and the conventional textiles is shown in  
340 Fig. 4f. The cooling performance distinction between the i-Cool (Cu) and the conventional textiles  
341 was still very apparent. To take a step further, we decreased skin power density of the artificial  
342 sweating skin to make skin temperature lower than ambient temperature to compare bare skin, i-  
343 Cool (Cu) and cotton, to see if the high thermal conductivity design in the i-Cool (Cu) will cause  
344 adverse effect for skin temperature. Consequently, skin temperature with the i-Cool (Cu) was  
345 almost the same as bare skin and showed better performance than cotton, as shown in  
346 Supplementary Fig. 21, indicating its evaporative cooling effect surpassed the opposing heat  
347 conduction from the ambient. In addition to high ambient temperature, we also investigated the  
348 performance of i-Cool (Cu) and other conventional textiles in a high relative humidity (RH)  
349 environment (Fig. 4g). As the relative humidity was raised, skin temperature with all the textile  
350 swatches rose correspondingly. Nevertheless, the skin temperature of the i-Cool (Cu) was still  
351 much lower than the conventional textiles.

352 Moreover, we performed measurements to see how the parameters in the functional structure  
353 design of i-Cool (Cu) influence its performance (See Supplementary Note 8 and Supplementary

354 Fig. 22 for more details). The results provide additional guidelines for personal perspiration  
355 management textile design.

### 356 **i-Cool practical application demonstration**

357 To further study the cooling effect of the i-Cool textile on human body, we developed a thermal  
358 simulation considering the coupled heat transfer, moisture vapor and liquid water transfer  
359 processes based on the actual human body with complex structure and dynamic physiological  
360 responses (See Supplementary Note 9, Supplementary Dataset 1 and Supplementary Fig. 23 for  
361 more details)<sup>49-51</sup>. The simulation results show that the i-Cool textile with improved evaporation  
362 ability and sweat evaporative cooling efficiency can achieve temperature reduction in both the skin  
363 temperature and core temperature of the human body compared to that with conventional textiles  
364 (Supplementary Fig. 23), which further validates the potential of the i-Cool structure design in  
365 efficient evaporative cooling for the human body.

366 To bridge the gap between i-Cool (Cu) concept demonstration to practical use, we demonstrated  
367 the feasibility via fabricating the i-Cool textile based on commercial fabrics. First, we verified the  
368 replacement of Cu matrix by polymer materials with heat conductive coatings. As shown in  
369 Supplementary Fig. 24, the i-Cool textiles using silver (Ag) coated polyester (PET) and  
370 nanoporous polyethylene (NanoPE) matrices exhibit almost the same performance as i-Cool (Cu)  
371 in the artificial sweating skin test (experimental parameters: same as Fig. 3d). Furthermore, we  
372 fabricated i-Cool textiles based on commercial knitted fabrics made of PET fibres. Here, we chose  
373 Dri-FIT and CoolMax which were already tested as control samples as the substrates. Figure 5a  
374 illustrates the fabrication process: holes were cut by laser cutting on the original fabric, after which  
375 it went through a facile electroless plating process. The Ag coating was deposited onto every  
376 fibre's surface of the fabric. Next, cellulose fibres were filled into the holes of the fabric, and  
377 prepared nylon 6 nanofibre film was transferred onto the fabric via press lamination to realize the  
378 i-Cool (Ag) textile which possessed the desired i-Cool structure. It is worthwhile to point out the  
379 fabrics we selected and the electroless plating method are not the only choices. Other textile  
380 material and other methods offering heat conductive coatings can be utilized. Alternatively, heat  
381 conductive fibres can be applied as well for the heat transport matrix. Figure 5b shows the  
382 photograph of the i-Cool (Ag) textile sample swatch (Dri-FIT as substrate). The photograph  
383 viewing from the i-Cool (Ag) bottom is exhibited in the inset of Fig. 5c, and the SEM images of

384 the Ag coated PET fibres (Fig. 5c, Supplementary Fig. 25) show the Ag coating is conformal and  
385 uniform. The branched structure formed in the electroless plating process can potentially enlarge  
386 evaporation area as well. The photograph and SEM images of i-Cool textile with CoolMax  
387 substrate are shown in Supplementary Fig. 26 and 27.

388 Successively, we performed the same steady-state evaporation test and artificial sweating skin test  
389 for the i-Cool (Ag) textile. In the steady-state evaporation test, the curves of i-Cool (Ag) plotted  
390 with curves of i-Cool (Cu), cotton and Dri-FIT (Fig. 5d and Fig. 5e) exhibited that i-Cool (Ag)  
391 exhibited very similar performance to the i-Cool (Cu) textile. Compared to the original Dri-FIT  
392 textile acting as the substrate, i-Cool (Ag) owns significantly improved evaporation performance  
393 and evaporative cooling efficiency, which is owing to the i-Cool functional structure. Also, in the  
394 artificial sweating skin test, i-Cool (Ag) and i-Cool (Cu) presented comparable cooling  
395 performance for personal perspiration management, which was significantly improved in contrast  
396 to cotton and Dri-FIT. This is also true for the i-Cool textile prepared with CoolMax substrate  
397 (Supplementary Fig. 28). With only sweat transportation channels, the modified Dri-FIT and  
398 CoolMax showed weaker cooling performance (Supplementary Fig. 28), which verifies the i-Cool  
399 structure combining heat conduction with water transportation provides superior strategy in  
400 personal perspiration management. These results demonstrate the feasibility of readily applying  
401 the i-Cool concept to practical usage.

402 In summary, we report a novel concept of i-Cool textile with unique functional structure design  
403 for personal perspiration management. The innovative employment of integrated water transport  
404 and heat conductive functional components together not only ensures its wicking ability, but also  
405 the fast evaporation rate, enhanced evaporative cooling effect and reduction of human body  
406 dehydration for human body via utilizing sweat in a highly efficient manner, which was  
407 demonstrated by the transient and steady-state evaporation test. An artificial sweating skin  
408 platform with feedback control loop simulating human body perspiration situation was realized,  
409 on which the i-Cool (Cu) textile shows comparable performance to the bare skin and apparent  
410 cooling effect with less provided sweat compared to the conventional textiles. Also, the structure  
411 advantage maintains under various conditions of exercise and ambient environment. Besides, the  
412 practical application feasibility of the i-Cool design principles was demonstrated, exhibiting decent

413 performance. Therefore, we expect the i-Cool textile will open a new door and provide new  
414 insights for the textiles for personal perspiration management.

415

## 416 **Methods**

417 **Textile preparation.** The Cu matrix used in the i-Cool (Cu) textile sample (main text) was  
418 prepared with Cu foil ( $\sim 25 \mu\text{m}$  thickness, Pred Materials) laser cut via DPSS UV laser cutter. A  
419 pore array (2 mm diameter, 3 mm pitch) on the Cu foil was created to realize the Cu matrix. Nylon  
420 6 nanofibre film was prepared by electrospinning. The nylon 6 solution system used in this work  
421 is 20 wt% nylon-6 (Sigma-Aldrich) in formic acid (Alfa Aesar). The polymer solution was loaded  
422 in a 5 mL syringe with a 22-gauge needle tip, which is connected to a voltage supply (ES30P-5W,  
423 Gamma High Voltage Research). The solution was pumped out of the needle tip using a syringe  
424 pump (Aladdin). The nanofibres were collected by a grounded copper foil (Pred Materials). The  
425 applied potential was 15 kV. The pumping rate was 0.1 mL/h. The distance between the needle tip  
426 and the collector is 20 cm. After collecting nylon 6 nanofibres of desired mass, the nylon 6  
427 nanofibre film ( $\sim 4.5 \text{ g/m}^2$ ,  $\sim 25 \mu\text{m}$  thickness) was transferred and laminated on the Cu matrix. A  
428 hydraulic press (MTI) was used to press nylon 6 nanofibres both into the holes and on the top of  
429 the Cu matrix. The fabricated i-Cool (Cu) was  $\sim 45 \mu\text{m}$  thick and  $107.7 \text{ g/m}^2$ . The varied  
430 parameters of the i-Cool (Cu) textile are shown in Supplementary Fig. 22. To fabricate the i-Cool  
431 (Ag) textile sample, same pore array as above was cut by laser cutter (Epilog Fusion M2 laser  
432 cutter) for the Dri-FIT or CoolMax textiles. Then, the fabric was cleaned and modified with  
433 polydopamine (PDA) coating for 2 h in an aqueous solution that consists of 2 g/L dopamine  
434 hydrochloride (Sigma Aldrich) and 10 mM Tris-buffer solution (pH 8.5, Teknova)<sup>52</sup>. For  
435 electroless plating of silver (Ag), the PDA-coated fabrics were then dipped into a 25 g/L  $\text{AgNO}_3$   
436 solution (99.9%, Alfa Aesar) for 30 min to form the Ag seed layer. After rinsing with deionized  
437 (DI) water, the fabric was immersed into the plating bath solution containing  $4.2 \text{ g L}^{-1} \text{Ag}(\text{NH}_3)_2^+$   
438 (made by adding 28%  $\text{NH}_3 \cdot \text{H}_2\text{O}$  dropwise into  $5 \text{ g L}^{-1} \text{AgNO}_3$  until the solution became clear  
439 again) and  $5 \text{ g L}^{-1}$  glucose (anhydrous, EMD Millipore Chemicals)<sup>53</sup> for 2 hours. Next, the fabric  
440 was turned over and placed into a new plating bath for another 2 hours. After drying, cellulose  
441 fibers were filled into the cut pores by extraction filtration of paper pulp. Then, nylon 6 nanofibre  
442 film ( $\sim 2\text{-}2.5 \text{ g/m}^2$ ) was added onto it by the same process described above. The as-prepared i-Cool



443 (Ag) (based on Dri-FIT) is  $\sim 175 \text{ g/m}^2$ . The one based on CoolMax is  $\sim 199 \text{ g/m}^2$ . The PET matrix  
444 ( $\sim 50 \text{ }\mu\text{m}$  thickness) and NanoPE matrix ( $\sim 25 \text{ }\mu\text{m}$  thickness) were prepared by laser cutting in the  
445 same way, and went through the same Ag coating process and nylon 6 nanofibre film lamination.  
446 The cotton textile sample was from a common short-sleeve T-shirt (100% cotton, single jersey  
447 knit,  $135 \text{ g/m}^2$ ,  $\sim 400 \text{ }\mu\text{m}$  thickness, Dockers). The Dri-FIT textile sample was from a regular Dri-  
448 FIT T-shirt (100% PET, single jersey knit,  $143 \text{ g/m}^2$ ,  $\sim 400 \text{ }\mu\text{m}$  thickness, Nike). The CoolMax  
449 textile sample was from a T-shirt made of 100% CoolMax Extreme polyester fibers (100% PET,  
450 single jersey knit,  $166 \text{ g/m}^2$ ,  $\sim 445 \text{ }\mu\text{m}$  thickness, purchased from Galls.com). The Coolswitch  
451 textile sample was from a Coolswitch T-shirt (91%PET/9% Elastane, French terry knit,  $140 \text{ g/m}^2$ ,  
452  $\sim 350 \text{ }\mu\text{m}$  thickness, Under Armour).

453 **Material characterization.** The optical microscope images were taken with an Olympus optical  
454 microscope. The SEM images were taken by a FEI XL30 Sirion SEM (5 kV) and a FEI Nova  
455 NanoSEM 450 (5 kV).

456 **Wicking rate measurement.** The wicking rate measurement method was based on AATCC 198  
457 with modification.  $5 \text{ cm} \times 5 \text{ cm}$  textile samples were prepared ahead.  $0.1 \text{ mL}$  of distilled water was  
458 placed on the simulated skin platform by pipette. Then textile samples were covered on the water,  
459 and the time of water reaching the circle of  $1.5 \text{ cm}$  in radius on the top surface of textile was  
460 recorded. Wicking rate was calculated using wicking area divided by wicking time.

461 **One-way water transport characterization.** A  $5 \text{ cm} \times 5 \text{ cm}$  textile sample was fixed onto an  
462 acrylic frame that had a  $4 \text{ cm} \times 4 \text{ cm}$  square hole. Camera was placed right above the frame or  
463 underneath the frame to shoot videos.  $20 \text{ }\mu\text{L}$  of deionized water was added onto one side of textile  
464 sample and the water transport process was filmed. The water spreading area was calculated by an  
465 image processing software (SketchAndCalc Area Caculator). We calculated the  $S_{inner}$ ,  $S_{outer}$  and  
466  $\mu$  at the testing time of  $15 \text{ s}$ .

467 **Thermal resistance measurement.** The cut bar method adapted from ASTM 5470 was used to  
468 measure thermal resistance. In this setup, eight thermocouples are inserted into the center of two  
469  $1 \text{ inch} \times 1 \text{ inch}$  copper reference bars to measure the temperature profiles along the top and bottom  
470 bar. A resistance heater generates a heat flux which flows through the top bar followed by the  
471 sample and then the bottom bar after which the heat is dissipated into a large heat sink. The entire

472 apparatus (top bar, sample, bottom bar) is wrapped in thermal insulation. A modest pressure of  
473 approximately 15 psi was applied at the top bar to reduce contact resistance, and no thermal grease  
474 was used due to the material porosity. The temperature profiles of the top and bottom copper bars  
475 are then used to determine both the heat flux and the temperature drop across the sample stack,  
476 which can derive the total thermal resistance ( $R_{TOT}$ ). Plotting the  $R_{TOT}$  versus the number of  
477 sample layers, the sample thermal resistance with contact thermal resistance between samples can  
478 be obtained from the slope of the line.

479 **Water vapour transmission property tests.** The upright cup testing procedure was based on  
480 ASTM E96 with modification. Medium bottles (100 mL; Fisher Scientific) were filled with 80ml  
481 of distilled water, and sealed with the textile samples using open-top caps and silicone gaskets  
482 (Corning). The exposed area of the textile was 3 cm in diameter. The sealed bottles were placed  
483 into an environmental chamber in which the temperature was held at 35°C and relative humidity  
484 was 30% ± 5%. The mass of the bottles and the samples was measured periodically. By dividing  
485 the reduced mass of the water by the exposed area of the bottle (3 cm in diameter), the water vapour  
486 transmission was calculated. The evaporative resistance measurement was based on ISO  
487 11092/ASTM F1868 with modification. A heater was used to generate stable heat flux mimicking  
488 the skin. A metal foam soaked with water was placed on the heater. A waterproof but vapour  
489 permeable film was covered on the top of the metal foam to protect the textile sample from contact  
490 with water. The whole device was thermally guarded. For different textile samples, we adjusted  
491 the heat flux to maintain the same skin temperature (35 °C) for all measurements. The ambient  
492 temperature was controlled by the water recirculation system at 35 °C, and the relative humidity  
493 was within 24 ± 4%. The evaporative resistance was calculated by  $R_{ef} = \frac{(P_s - P_a) \cdot A}{H} - R_{ebp}$ , where  
494  $P_s$  is the water vapour pressure at the plate surface, which can be assumed as the saturation at the  
495 temperature of the surface,  $P_a$  is the water vapour pressure in the air,  $A$  is the area of the plate test  
496 section,  $H$  is the power input, and  $R_{ebp}$  is the value measured without any textile samples.

497 **Water vapour thermal measurement.** The artificial sweating skin platform was utilized in this  
498 measurement. A steady power density (580 W/m<sup>2</sup>) and water flow rate (0.25 mL/h) were adopted.  
499 An acrylic frame (thickness: 1.5mm) with a crossing was laser cut and placed on the platform to  
500 support the textile samples avoiding the liquid water contact. Stable skin temperature was read.  
501 The ambient was 22 °C ± 0.2 °C, 40% ± 5% relative humidity.

502 **Transient droplet evaporation test.** The skin was simulated by a polyimide insulated flexible  
503 heater (McMaster-Carr, 25 cm<sup>2</sup>) which was connected to a power supply (Keithley 2400). A ribbon  
504 type hot junction thermocouple (~ 0.1 mm in diameter, K-type, Omega) was in contact with the  
505 top surface of the simulated skin to measure the skin temperature. The heater was set on a 10 cm-  
506 thick foam for heat insulation. During the tests, water (37 °C) was added onto the simulated skin  
507 and textile samples were covered on the simulated skin immediately. The skin temperatures with  
508 wet textile samples during water evaporation were measured with an assorted combination of  
509 initial water amount and generated area power density of simulated skin. The average evaporation  
510 rate was calculated by dividing the initial water amount by evaporation time. The end point of the  
511 evaporation was defined as the inflection point between the relatively stable range and the rapid  
512 increase stage of temperature. The average skin temperature referred to the average temperature  
513 reading spanned the evaporation stage in which skin temperature was relatively stable. The mass  
514 of wet textile samples was measured by a digital balance (U. S. Solid, 0.001g accuracy) to track  
515 the water mass loss during the evaporation. The tests were all performed in an environment of  
516 22 °C ± 0.2 °C, 40% ± 5% relative humidity.

517 **Steady-state evaporation test.** The skin was simulated by a polyimide insulated flexible heater  
518 (McMaster-Carr, 25 cm<sup>2</sup>) which was connected to a power supply (Keithley 2400). It was covered  
519 by a 1.5 mm-thick acrylic board with grooves made by laser cutting (Epilog Fusion M2 laser cutter)  
520 on its top surface. A ribbon type hot junction thermocouple (~ 0.1 mm in diameter, K-type, Omega)  
521 was sealed in a groove by PDMS to measure the skin temperature. A needle connected to a tube  
522 and a syringe pump (Harvard, PHD 2000) was also sealed in one groove of the acrylic board, but  
523 with head exposed for water outage. The heater was set on a 10 cm-thick foam for heat insulation.  
524 During the tests, water in the tube was heated by a proportional–integral–derivative (PID)  
525 temperature controller (Omega Engineering) at 37 °C before flowing onto the artificial skin.  
526 Textile samples were placed on the artificial skin surface. The applied power density was adjusted  
527 to let measured skin temperature fluctuate around 35 °C. After stabilization for a period of time,  
528 the mass of wet textile samples was measured by a digital balance (U. S. Solid, 0.001g accuracy),  
529 and power density was recorded. The tests were all performed in an environment of 19.5 °C ±  
530 0.3 °C, 35% ± 5% relative humidity.

531 **Fabrication of Janus-type wicking layer with limited water outlets.** A filter paper (Qualitative,  
532 Whatman) was used as the wicking layer. An acrylic board was laser cut into a mask with Epilog  
533 Fusion M2 Laser and placed on the top of the filter paper. Polydimethylsiloxane (PDMS) base and  
534 curing agent (Sylgard 184, Dow Corning) with mass ratio 10: 1 were dispersed into hexane (Fisher  
535 Scientific) with volume ratio 1: 10. The PDMS solution was sprayed onto the masked filter paper  
536 that was on a heating plate, which helped with faster volatilization of hexane. After drying and  
537 curing, the PDMS formed hydrophobic coating layer only on the uncovered place of the top surface  
538 of the filter paper, which could absorb and transport water from the bottom surface but provide  
539 limited water outlets on the top surface.

540 **Artificial sweating skin test with feedback control loop.** The water reservoir (5 cm × 5 cm × 2.5  
541 mm) with water inlet (whole part size: 8 cm × 8 cm × 3.5 mm) was made by 3D printing  
542 (FlashForge Creator Pro). A cover with a 9 × 9 hole (diameter: 3 mm) array (hole array area: 5 cm  
543 × 5 cm, whole part size: 8 cm × 8 cm × 1.5 mm) was also 3D printed and bound with the water  
544 reservoir part. The water reservoir was connected to a syringe pump (Harvard, PHD 2000). The  
545 pumped water was heated at 37 °C by a heater (Omega Engineering) and a proportional–integral–  
546 derivative (PID) temperature controller (Omega Engineering). A polyimide insulated flexible  
547 heater (McMaster-Carr, 25 cm<sup>2</sup>) with laser cut water outlets was adhered to the holey cover. The  
548 heater was connected to a power supply (Keithley 2400). Then, the fabricated Janus-type wicking  
549 layer with limited water outlets was attached to the heater layer to serve as the skin surface. A  
550 ribbon type hot junction thermocouple (~ 0.1 mm in diameter, K-type, Omega) connected to a  
551 thermocouple meter (Omega Engineering) was in contact with the top surface of the Janus-type  
552 wicking layer to measure the skin temperature. The thermocouple meter, syringe pump and power  
553 supply were all controlled by a LabView program, which can alter the pumping rate (extra  
554 sweating rate) according to the thermometer reading (skin temperature) in real time. Before the  
555 test, the artificial sweating skin platform was filled with water in advance. The perspiration  
556 threshold skin temperature was set to be 34.5 °C, over which the sweating rate was linearly  
557 dependent on skin temperature<sup>47,48</sup>. The relationship between pumping rate and skin temperature  
558 was set as pumping rate (mL/h) = 0.32\*skin temperature (°C) - 11.04, which was decided  
559 according to previous research and reasonable human body perspiration rate range. The whole set-  
560 up was in a space without forced convection. No chamber with cover for the set-up was used to

561 avoid water vapour accumulation except the high-humidity test. In the high-humidity test, a  
562 humidifier was placed next to the testing platform and they are enclosed together to change the  
563 humidity. The initial air temperature in the chamber was 22 °C but about 1-2 °C reading variation  
564 of the ambient temperature thermometer was observed, perhaps due to the water vapour  
565 condensation, but no obvious influence on the skin temperature was observed. In other cases, if no  
566 ambient temperature and relative humidity are specified, the ambient temperature was 22 °C ±  
567 0.2 °C and ambient relative humidity was 40% ± 5%.

568

### 569 **Data Availability**

570 The data that support the findings of this study are available from the corresponding author upon  
571 reasonable request.

572

### 573 **Code Availability**

574 The code for thermal simulation of actual human body is available from the corresponding author  
575 upon reasonable request.

576

### 577 **References**

- 578 1. Kjellstrom, T. *et al.* Heat, Human Performance, and Occupational Health: A Key Issue for  
579 the Assessment of Global Climate Change Impacts. *Annu. Rev. Public Health* **37**, 97–112  
580 (2016).
- 581 2. Goldstein, L. S., Dewhirst, M. W., Repacholi, M. & Kheifets, L. Summary, conclusions  
582 and recommendations: Adverse temperature levels in the human body. *Int. J. Hyperth.* **19**,  
583 373–384 (2003).
- 584 3. Chan, A. P. C. & Yi, W. Heat stress and its impacts on occupational health and  
585 performance. *Indoor Built Environ.* **25**, 3–5 (2016).
- 586 4. Hsu, P.-C. *et al.* Personal Thermal Management by Metallic Nanowire-Coated Textile.

- 587 *Nano Lett.* **15**, 365–371 (2015).
- 588 5. Tong, J. K. *et al.* Infrared-Transparent Visible-Opaque Fabrics for Wearable Personal  
589 Thermal Management. *ACS Photonics* **2**, 769–778 (2015).
- 590 6. Raman, A. P., Anoma, M. A., Zhu, L., Rephaeli, E. & Fan, S. Passive radiative cooling  
591 below ambient air temperature under direct sunlight. *Nature* **515**, 540–544 (2014).
- 592 7. Li, W., Shi, Y., Chen, Z. & Fan, S. Photonic thermal management of coloured objects.  
593 *Nat. Commun.* **9**, 1–8 (2018).
- 594 8. Zhang, X. A. *et al.* Dynamic gating of infrared radiation in a textile. *Science (80-. )*. **363**,  
595 619–623 (2019).
- 596 9. Peng, Y. & Cui, Y. Advanced Textiles for Personal Thermal Management and Energy.  
597 *Joule* **4**, 724–742 (2020).
- 598 10. Hardy, J. D. & DuBois, E. F. Regulation of Heat Loss from the Human Body. *Proc. Natl.*  
599 *Acad. Sci.* **23**, 624–631 (1937).
- 600 11. Hsu, P.-C. *et al.* Radiative human body cooling by nanoporous polyethylene textile.  
601 *Science (80-. )*. **353**, 1019–1023 (2016).
- 602 12. Hsu, P.-C. *et al.* A dual-mode textile for human body radiative heating and cooling. *Sci.*  
603 *Adv.* **3**, e1700895 (2017).
- 604 13. Peng, Y. *et al.* Nanoporous polyethylene microfibrils for large-scale radiative cooling  
605 fabric. *Nat. Sustain.* **1**, 105–112 (2018).
- 606 14. Cai, L. *et al.* Warming up human body by nanoporous metallized polyethylene textile.  
607 *Nat. Commun.* **8**, 496 (2017).
- 608 15. Cai, L. *et al.* Spectrally Selective Nanocomposite Textile for Outdoor Personal Cooling.  
609 *Adv. Mater.* **30**, 1802152 (2018).
- 610 16. Cai, L. *et al.* Temperature Regulation in Colored Infrared-Transparent Polyethylene  
611 Textiles. *Joule* **3**, 1478–1486 (2019).
- 612 17. Gao, T. *et al.* Three-Dimensional Printed Thermal Regulation Textiles. *ACS Nano* **11**,

- 613 11513–11520 (2017).
- 614 18. Cui, Y., Gong, H., Wang, Y., Li, D. & Bai, H. A Thermally Insulating Textile Inspired by  
615 Polar Bear Hair. *Adv. Mater.* **30**, 1706807 (2018).
- 616 19. Zhao, M. *et al.* A study on local cooling of garments with ventilation fans and openings  
617 placed at different torso sites. *Int. J. Ind. Ergon.* **43**, 232–237 (2013).
- 618 20. Katić, K., Li, R. & Zeiler, W. Thermophysiological models and their applications: A  
619 review. *Build. Environ.* **106**, 286–300 (2016).
- 620 21. Kuno, Y. *HUMAN PERSPIRATION*. By Kuno, Yas. Springfield, Illinois: Charles C.  
621 Thomas. Blackwell Scientific Publications: Oxford. 1956. Pp. xv + 417. 72s. (Charles C  
622 Thomas, 1957). doi:10.1113/expphysiol.1957.sp001275.
- 623 22. Nielsen, B. Regulation of Body Temperature and Heat Dissipation at Different Levels of  
624 Energy-and Heat Production in Man. *Acta Physiol. Scand.* **68**, 215–227 (1966).
- 625 23. Mack, G. W. & Nadel, E. R. Body Fluid Balance During Heat Stress in Humans. in  
626 *Comprehensive Physiology* (2011). doi:10.1002/cphy.cp040110.
- 627 24. Angelova, R. A., Reiners, P., Georgieva, E. & Kyosev, Y. The effect of the transfer  
628 abilities of single layers on the heat and mass transport through multilayered outerwear  
629 clothing for cold protection. *Text. Res. J.* **88**, 1125–1137 (2018).
- 630 25. Davis, J. K. & Bishop, P. A. Impact of clothing on exercise in the heat. *Sport. Med.* **43**,  
631 695–706 (2013).
- 632 26. Scheurell, D. M., Spivak, S. M. & Hollies, N. R. S. Dynamic Surface Wetness of Fabrics  
633 in Relation to Clothing Comfort. *Text. Res. J.* **55**, 394–399 (1985).
- 634 27. Gavin, T. P. Clothing and Thermoregulation during exercise. in *Textiles and the Skin* vol.  
635 31 35–49 (KARGER, 2003).
- 636 28. Varshney, R. K., Kothari, V. K. & Dhamija, S. A study on thermophysiological comfort  
637 properties of fabrics in relation to constituent fibre fineness and cross-sectional shapes. *J.*  
638 *Text. Inst.* **101**, 495–505 (2010).
- 639 29. Hu JY, Li YI, Y. K. No Title. in *Clothing biosensory engineering*. (ed. Li Y, W. A.) 229–

- 640 231 (Cambridge: Woodhead, 2006).
- 641 30. Senthilkumar, M., Sampath, M. B. & Ramachandran, T. Moisture Management in an  
642 Active Sportswear: Techniques and Evaluation—A Review Article. *J. Inst. Eng. Ser. E*  
643 **93**, 61–68 (2012).
- 644 31. Nazir, A., Hussain, T., Abbas, G. & Ahmed, A. Effect of Design and Method of Creating  
645 Wicking Channels on Moisture Management and Air Permeability of Cotton Fabrics. *J.*  
646 *Nat. Fibers* **12**, 232–242 (2015).
- 647 32. Wang, Y. *et al.* Reversible Water Transportation Diode: Temperature-Adaptive Smart  
648 Janus Textile for Moisture/Thermal Management. *Adv. Funct. Mater.* **30**, 1–9 (2020).
- 649 33. Lao, L., Shou, D., Wu, Y. S. & Fan, J. T. “Skin-like” fabric for personal moisture  
650 management. *Sci. Adv.* **6**, 1–12 (2020).
- 651 34. Dai, B. *et al.* Bioinspired Janus Textile with Conical Micropores for Human Body  
652 Moisture and Thermal Management. *Adv. Mater.* **31**, (2019).
- 653 35. Dong, Y. *et al.* Tailoring surface hydrophilicity of porous electrospun nanofibers to  
654 enhance capillary and push-pull effects for moisture wicking. *ACS Appl. Mater. Interfaces*  
655 **6**, 14087–14095 (2014).
- 656 36. Sarkar, M., Fan, J., Szeto, Yu C. & Tao, X. Biomimetics of Plant Structure in Textile  
657 Fabrics for the Improvement of Water Transport Properties. *Text. Res. J.* **79**, 657–668  
658 (2009).
- 659 37. Wang, X. *et al.* Biomimetic Fibrous Murray Membranes with Ultrafast Water Transport  
660 and Evaporation for Smart Moisture-Wicking Fabrics. *ACS Nano* acsnano.8b08242 (2018)  
661 doi:10.1021/acsnano.8b08242.
- 662 38. Craig, F. N. & Moffitt, J. T. Efficiency of evaporative cooling from wet clothing. *J. Appl.*  
663 *Physiol.* **36**, 313–316 (1974).
- 664 39. Havenith, G. *et al.* Evaporative cooling: Effective latent heat of evaporation in relation to  
665 evaporation distance from the skin. *J. Appl. Physiol.* **114**, 778–785 (2013).
- 666 40. Guan, M. *et al.* Apparent evaporative cooling efficiency in clothing with continuous



- 667 perspiration: A sweating manikin study. *Int. J. Therm. Sci.* **137**, 446–455 (2019).
- 668 41. Campbell, I. Body temperature and its regulation. *Anaesth. Intensive Care Med.* **12**, 240–  
669 244 (2011).
- 670 42. Jiao, J. *et al.* Effects of body-mapping-designed clothing on heat stress and running  
671 performance in a hot environment. *Ergonomics* **60**, 1435–1444 (2017).
- 672 43. Wilke, K. L., Barabadi, B., Lu, Z., Zhang, T. & Wang, E. N. Parametric study of thin film  
673 evaporation from nanoporous membranes. *Appl. Phys. Lett.* **111**, 171603 (2017).
- 674 44. Hanks, D. F. *et al.* High Heat Flux Evaporation of Low Surface Tension Liquids from  
675 Nanoporous Membranes. *ACS Appl. Mater. Interfaces* **12**, 7232–7238 (2020).
- 676 45. Yao, B. guo, Li, Y., Hu, J. yan, Kwok, Y. lin & Yeung, K. wing. An improved test method  
677 for characterizing the dynamic liquid moisture transfer in porous polymeric materials.  
678 *Polym. Test.* **25**, 677–689 (2006).
- 679 46. Kuht, J. & Farmery, A. D. Body temperature and its regulation. *Anaesth. Intensive Care*  
680 *Med.* **19**, 507–512 (2018).
- 681 47. Nadel, E. R., Bullard, R. W. & Stolwijk, J. A. Importance of skin temperature in the  
682 regulation of sweating. *J. Appl. Physiol.* **31**, 80–87 (1971).
- 683 48. McCaffrey, T. V., Wurster, R. D., Jacobs, H. K., Euler, D. E. & Geis, G. S. Role of skin  
684 temperature in the control of sweating. *J. Appl. Physiol.* **47**, 591–597 (1979).
- 685 49. li, Y. & Holcombe, B. V. Mathematical Simulation of Heat and Moisture Transfer in a  
686 Human-Clothing-Environment System. *Text. Res. J.* (1998)  
687 doi:10.1177/004051759806800601.
- 688 50. Li, F., Li, Y. & Wang, Y. A 3D finite element thermal model for clothed human body. *J.*  
689 *Fiber Bioeng. Informatics* **6**, 149–160 (2013).
- 690 51. Zhu, Q. Y. & Li, Y. A model of coupled liquid moisture and heat transfer in porous  
691 textiles with consideration of gravity. *Numerical Heat Transfer, Part A*, **43**, 501–523  
692 (2003)
- 693 52. Lee, H., Dellatore, S. M., Miller, W. M. & Messersmith, P. B. Mussel-Inspired Surface

694 Chemistry for Multifunctional Coatings. *Science* (80-. ). **318**, 426–430 (2007).  
695 53. Hsu, P.-C. *et al.* Electrolessly Deposited Electrospun Metal Nanowire Transparent  
696 Electrodes. *J. Am. Chem. Soc.* **136**, 10593–10596 (2014).

697

## 698 **Acknowledgements**

699 The authors acknowledge the great help of P. Zhu, C. Lau, G. Gerboni, Z. Yu and Y. Zheng. Part  
700 of this work was performed at the Stanford Nano Shared Facilities and the Stanford  
701 Nanofabrication Facility. J.S., C.D., and R.P. acknowledge the support of the Laboratory Directed  
702 Research and Development Program (LDRD) at Lawrence Berkeley National Laboratory under  
703 contract # DE-AC02-05CH11231.

704

## 705 **Author Contributions**

706 Y. C. and Y. P. conceived the idea. Y. P. designed and conducted the experiments. Y. P., W. L.  
707 and B. L. performed the feedback control loop construction and programming. W. L. and W. J.  
708 conducted the simulation. B. L. drew the schematics. J. T. and G. Z. helped with sample  
709 preparation. J. S. and J. Z. performed the thermal resistance measurement. G. W. helped with  
710 statistical analysis. Y. Z and C. Z. helped with laser cutting process. W. H. and T. W. provided  
711 helpful discussion. Y. C. and R. P., C. D., S.F., K. G. supervised the project. All the authors  
712 provided helpful discussion on this project and contributed to manuscript writing.

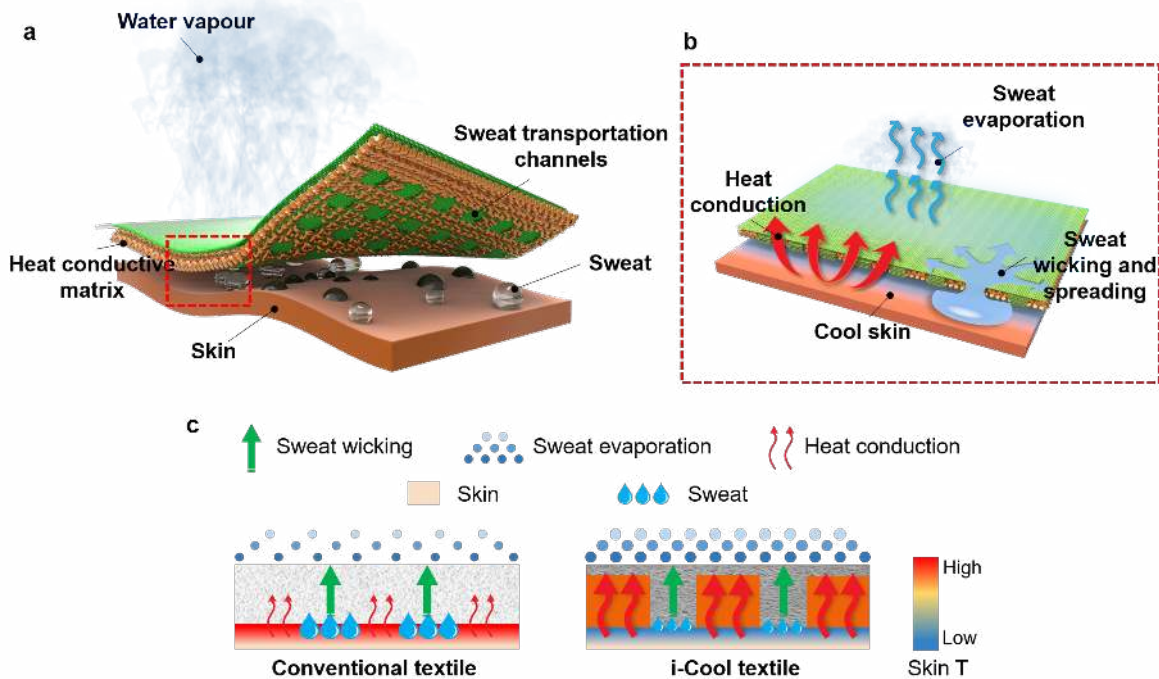
713

## 714 **Competing Interests**

715 The authors declare no competing interests.

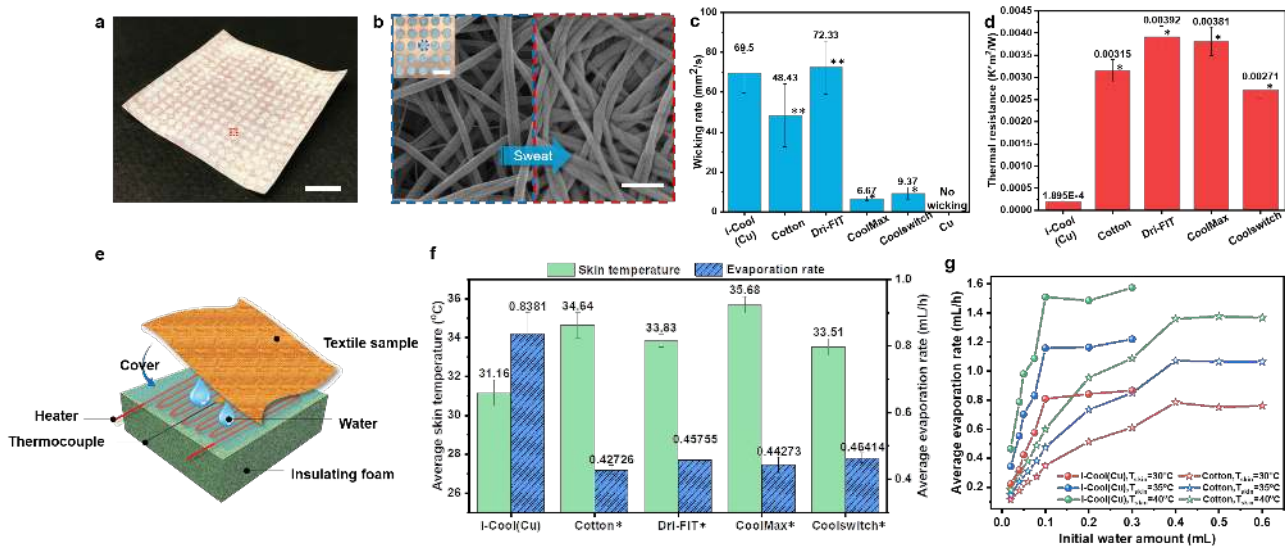
716

717



719

720 **Figure 1. Schematic of the functional structure design of integrated cooling (i-Cool) textile**  
 721 **of heat conduction and sweat transportation for personal perspiration management and its**  
 722 **working mechanism. a,** Schematic of the i-Cool textile. The synergistic effect of the heat  
 723 conductive matrix and sweat transport channels provides a solution to textile in personal  
 724 perspiration management. **b,** Schematic of the working mechanism of the i-Cool textile. When  
 725 human body perspires, the water transport channels can wick sweat from the skin surface and  
 726 spread sweat onto the large-area top surface made of fibres quickly. The heat conductive matrix  
 727 transfers human body heat efficiently to where the evaporation happens, to assist fast evaporation.  
 728 Meanwhile, it can deliver the evaporative cooling effect to human body skin efficiently. **c,**  
 729 Comparison between conventional textiles and the i-Cool textile. Conventional textiles usually  
 730 offer comfort via buffer effect of absorbing sweat, which is helpful to relieve discomfort of wet  
 731 and sticky sense. However, its limited evaporation rate and evaporative cooling efficiency cannot  
 732 provide effective cooling effect for skin and may undermine the buffer effect soon. Different from  
 733 normal textiles, the i-Cool textile functions not only to transport sweat but also provide an excellent  
 734 heat conduction path for the accelerated evaporation and taking away a great amount of heat from  
 735 the skin, which can prevent the i-Cool textile from flooding to a much greater extent and avoid  
 736 excessive perspiration. Therefore, the i-Cool textile can help human body achieve enhanced  
 737 cooling effect, by greatly reduced sweat consumed and by using the sweat in a highly efficient  
 738 manner. The weight contrast in red arrows drawing illustrates the heat transport ability difference.  
 739 The dot size and density contrast in the sweat evaporation drawing shows the different evaporation  
 740 ability. The drop size contrast in the sweat drawing illustrates that i-Cool textile can help reduce  
 741 sweat consumption.



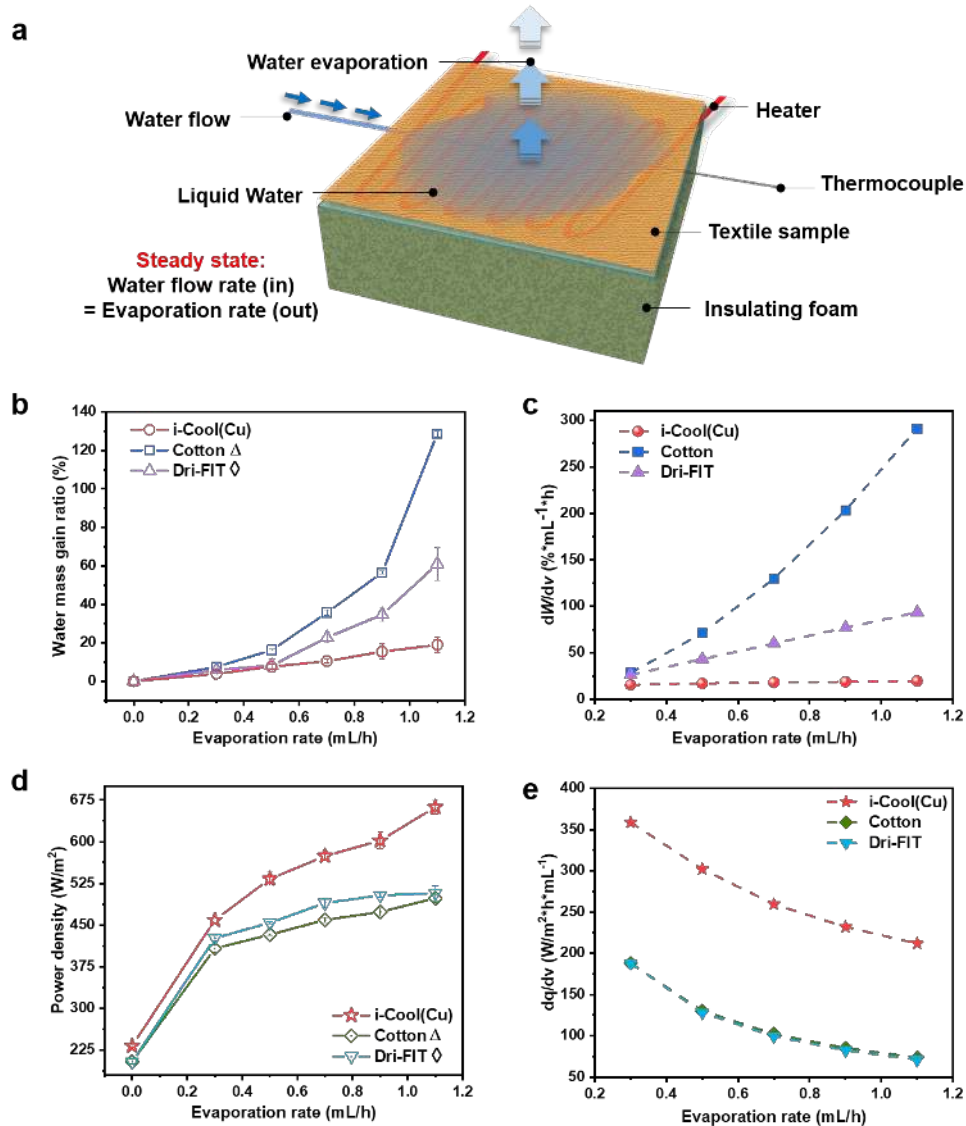
742 **Figure 2. Wicking performance, thermal resistance and transient droplet evaporation test of**  
 743 **the i-Cool (Cu) textile.** **a**, Photograph of as-prepared i-Cool (Cu) textile. Scale bar, 1 cm. **b**, SEM  
 744 image of nylon 6 nanofibres in the pores of heat conductive matrix (blue dash box) and on the top  
 745 of heat conductive matrix skeleton (red dash box). Sweat tends to be transported to the nanofibres  
 746 on the heat conductive matrix skeleton due to the morphology difference. Scale bar, 1  $\mu$ m. Inset is  
 747 the magnified photograph of the bottom side of i-Cool (Cu) textile showing its integrated heat  
 748 conduction channels and water transport channels. The holes are 2 mm in diameter and 3 mm pitch.  
 749 Scale bar, 4 mm. **c**, Wicking rate of the i-Cool (Cu), cotton and other commercial textiles. It shows  
 750 how fast water underneath the textile can be pulled up and spread on the top surface. Double  
 751 asterisks, Statistical significance between the i-Cool (Cu) and labelled sample, Welch's t-test  $p <$   
 752  $0.1$ ; Asterisk, Statistical significance between the i-Cool (Cu) and labelled sample, Welch's t-test  
 753  $p < 0.001$ . **d**, Thermal resistance of the i-Cool (Cu), cotton and other commercial textiles measured  
 754 by cut-bar method (See more discussion in Supplementary Note 2). Asterisk, Statistical  
 755 significance between the i-Cool (Cu) and labelled sample, Welch's t-test  $p < 0.001$ . **e**, Schematic  
 756 illustration of the transient droplet evaporation test. **f**, Average skin temperature and average  
 757 evaporation rate of the i-Cool (Cu) textile and the conventional textiles (initial water amount: 0.1  
 758 mL, skin heater power density: 422.5 W/m<sup>2</sup>). Asterisk, Statistical significance of average skin  
 759 temperature between the i-Cool (Cu) textile and other textile samples, Welch's t-test  $p < 0.001$ .  
 760 Statistical significance of average evaporation rate between the i-Cool (Cu) textile and other textile  
 761 samples, Welch's test  $p < 0.001$ . **g**, Fitted average evaporation rate of i-Cool (Cu) and cotton versus  
 762 initial water amount at different skin temperature. All the error bars represent standard deviation  
 763 of measured data.

764

765

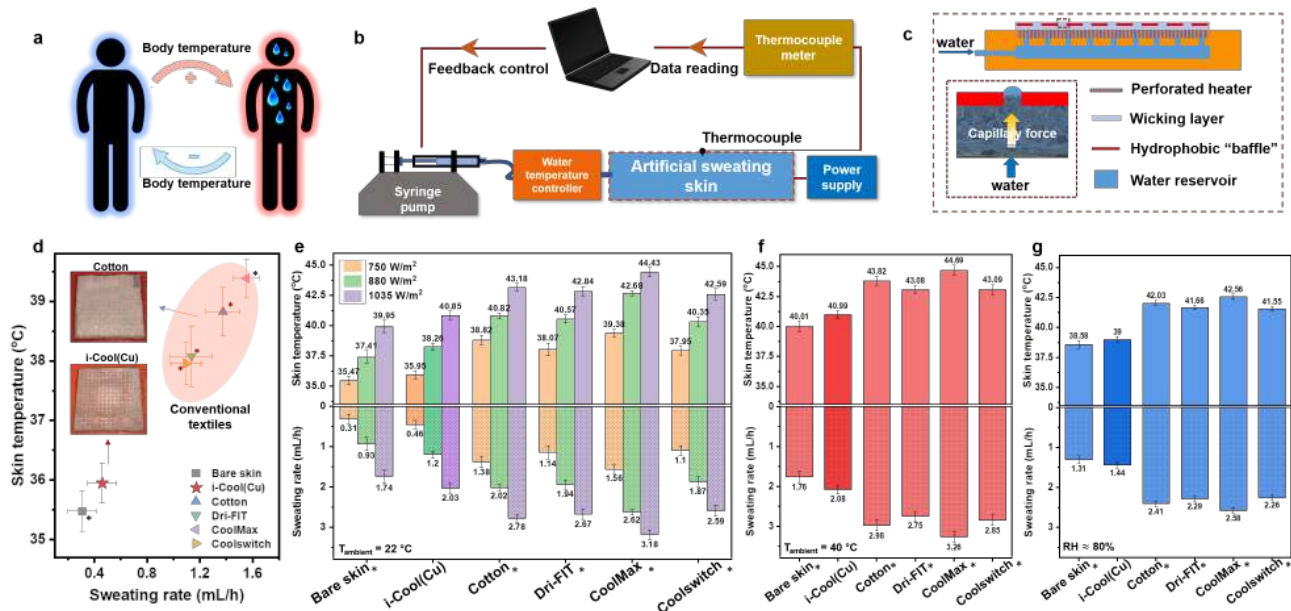
766

767



768

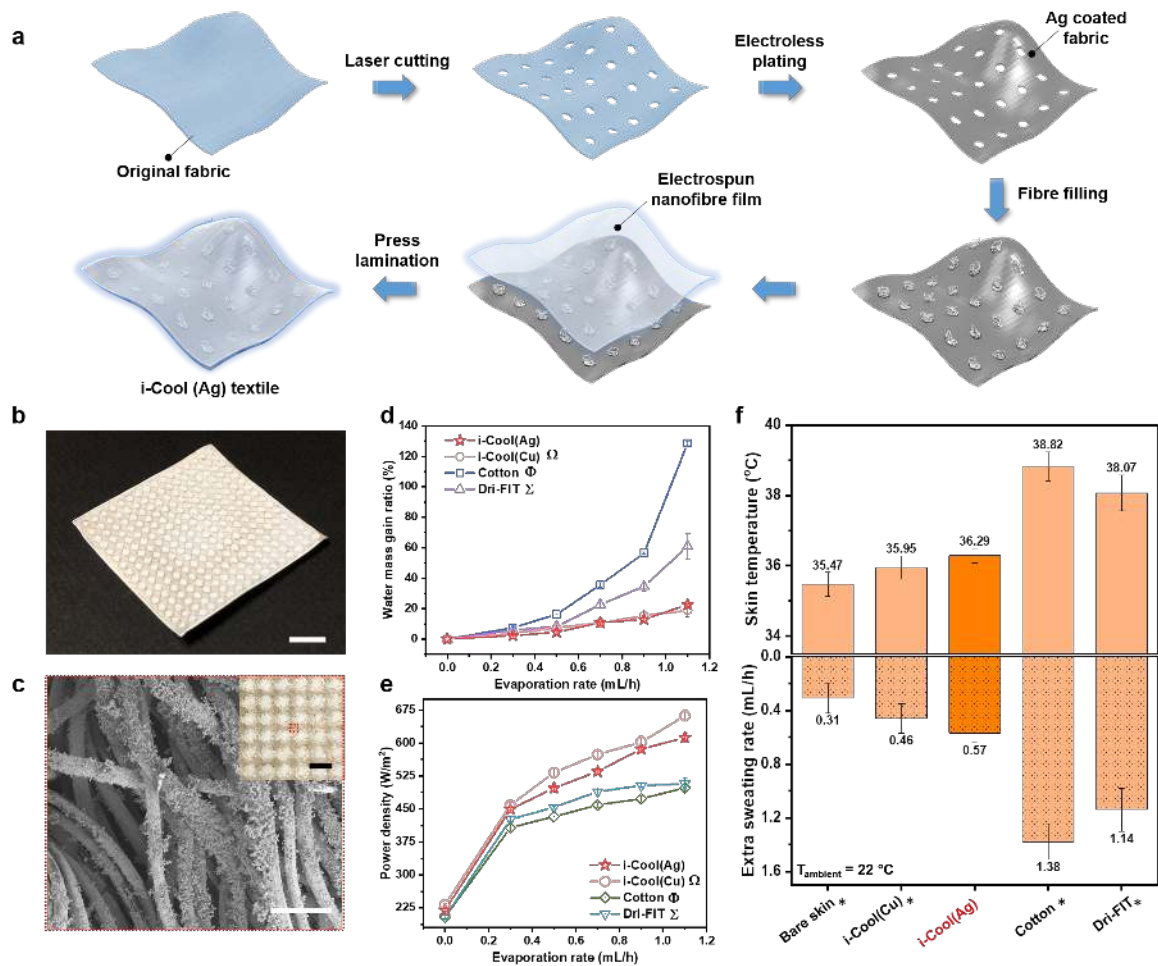
769 **Figure 3. Steady-state evaporation test of the i-Cool (Cu) textile, cotton and Dri-FIT.** **a**,  
 770 Schematic illustration of the measurement apparatus and method. **b**, Measured water mass gain  
 771 ratio ( $W$ ) at different evaporation rate ( $v$ ). Triangle, Statistical significance between the i-Cool (Cu)  
 772 and cotton, Welch's t-test  $p < 0.1$  at 0.3 mL/h,  $p < 0.001$  at 0.7 mL/h,  $p < 0.01$  for others. Diamond,  
 773 Statistical significance between the i-Cool (Cu) and Dri-FIT, Welch's test  $p < 0.05$  at 0.3 mL/h,  
 774 no statistical significance at 0.5 mL/h,  $p < 0.01$  for others. **c**,  $dW/dv$  obtained by fitting data in (b).  
 775 i-Cool (Cu) can achieve a certain evaporation rate with much lower water gain. The required water  
 776 gain increase for larger evaporation rate is also reduced. **d**, Measured power density ( $q$ ) at different  
 777 evaporation rate ( $v$ ). Triangle, Statistical significance between the i-Cool (Cu) and cotton, Welch's  
 778 t-test  $p < 0.05$  at 0.3 mL/h,  $p < 0.001$  at 0.7 mL/h, 0.9 mL/h,  $p < 0.01$  for others. Diamond,  
 779 Statistical significance between the i-Cool (Cu) and Dri-FIT, Welch's test shows no statistical  
 780 significance at 0.3 mL/h,  $p < 0.05$  at 0.5 mL/h,  $p < 0.01$  at 0.7 mL/h, 0.9 mL/h,  $p < 0.001$  for others.  
 781 **e**,  $dq/dv$  obtained by fitting data in (d). The i-Cool (Cu) can show enhanced cooling effect with  
 782 higher sweat evaporative cooling efficiency. All the error bars represent standard deviation of  
 783 measured data.



784 **Figure 4. Artificial sweating skin platform with feedback control loop and measurements on**  
 785 **it. a**, Schematic of human body temperature self-regulation mechanism. When body temperature  
 786 increases, human body perspires to cool down its own temperature, which leads to reduction or  
 787 suspension of perspiration in reverse. **b**, Schematic of the artificial sweating skin platform with  
 788 feedback control loop simulating human body temperature self-regulation mechanism. **c**,  
 789 Schematic of the detailed structure of the artificial sweating skin. The schematic in the red dash  
 790 box shows the working mechanism of the modified Janus-type wicking layer which realizes  
 791 uniform sweating mimicking human skin sweating scenario. **d**, Measurement results of skin  
 792 temperature and sweating rate for bare skin, i-Cool (Cu) and commercial textiles (skin power  
 793 density: 750 W/m<sup>2</sup>, ambient temperature: 22 °C). Insets show the photographs of i-Cool (Cu) and  
 794 cotton after one-hour stabilization during the tests. Asterisk, Statistical significance of skin  
 795 temperature and sweating rate between the i-Cool (Cu) and other textiles, Welch's t-test  $p < 0.001$ .  
 796 **e**, Measurement results of skin temperature and sweating rate for bare skin, i-Cool (Cu) and other  
 797 conventional textiles under different skin power densities. Asterisk, Statistical significance of skin  
 798 temperature and sweating rate between the i-Cool (Cu) and other textiles at 750 W/m<sup>2</sup>, 880 W/m<sup>2</sup>  
 799 and 1035 W/m<sup>2</sup>, Welch's t-test  $p < 0.001$ . **f**, Measured skin temperature and sweating rate at high  
 800 ambient temperature (40 °C). 750 W/m<sup>2</sup> power density was applied. Asterisk, Statistical  
 801 significance of skin temperature and sweating rate between the i-Cool (Cu) and other textiles,  
 802 Welch's t-test  $p < 0.001$ . **g**, Measured skin temperature and sweating rate in high relative humidity  
 803 ambient (~80%). Asterisk, Statistical significance of skin temperature and sweating rate between  
 804 the i-Cool (Cu) and other textiles, Welch's t-test  $p < 0.001$ . All the error bars represent standard  
 805 deviation of measured data.

806

807



808  
809 **Figure 5. Practical application feasibility demonstration of the i-Cool functional structure**  
810 **via i-Cool (Ag) textile.** **a**, Illustration of the fabrication process of i-Cool (Ag) textile based on a  
811 commercially available fabric. **b**, Photograph of as-fabricated i-Cool (Ag) textile based on Dri-FIT  
812 as the substrate. Scale bar, 1 cm. **c**, SEM image showing the uniform and conformal Ag coating  
813 on the PET fibres of the fabric substrate. Scale bar, 50  $\mu\text{m}$ . The inset shows the photograph of i-  
814 Cool (Ag) viewing from its bottom. Scale bar, 4 mm. **d**, Measured water mass gain ratio of i-Cool  
815 (Ag) and other textiles at different evaporation rate in the steady-state evaporation test. Omega  
816 symbol, Statistical significance between the i-Cool (Ag) and i-Cool (Cu), Welch's t-test  $p < 0.1$  at  
817 0.3 mL/h and 0.5 mL/h, no statistical significance for others. Phi symbol, Statistical significance  
818 between the i-Cool (Ag) and cotton, Welch's test  $p < 0.05$  at 0.3 mL/h,  $p < 0.001$  for others. Sigma  
819 symbol, Statistical significance between the i-Cool (Ag) and Dri-FIT, Welch's test shows no  
820 statistical significance at 0.5 mL/h,  $p < 0.05$  at 0.7 mL/h, 1.1 mL/h,  $p < 0.01$  for others. **e**, Measured  
821 power density of i-Cool (Ag) and other textiles at different evaporation rate in the steady-state  
822 evaporation test. Omega symbol, Statistical significance between the i-Cool (Ag) and i-Cool (Cu),  
823 Welch's t-test  $p < 0.01$  at 0 mL/h, 1.1 mL/h,  $p < 0.05$  at 0.7 mL/h, no statistical significance for  
824 others. Phi symbol, Statistical significance between the i-Cool (Ag) and cotton, Welch's test  $p <$   
825  $0.001$  at 0.7 mL/h and 0.9 mL/h,  $p < 0.01$  for others. Sigma symbol, Statistical significance  
826 between the i-Cool (Ag) and Dri-FIT, Welch's test  $p < 0.05$  at 0.5 mL/h,  $p < 0.01$  at 0.3 mL/h and  
827 0.7 mL/h,  $p < 0.001$  for others. **f**, Measured skin temperature and sweating rate of the i-Cool (Ag)  
828 textile on the artificial sweating skin platform with feedback control loop. Asterisk, Statistical

829 significance of skin temperature and sweating rate between the i-Cool (Ag) and other textiles,  
830 Welch's t-test  $p < 0.001$ . All the error bars represent standard deviation of measured data.  
831